Flexural Performance of Seawater-Mixed Recycled-Aggregate GFRP-Reinforced Concrete Beams

Adel Younis[1], Usama Ebead[2*], Prannoy Suraneni[3], and Antonio Nanni[4]

[1] Ph.D. Candidate, Department of Civil and Architectural Engineering, College of Engineering, Qatar University, P.O. Box 2713, Doha, Qatar, e–mail: adel.younis@qu.edu.qa

[2] Professor of Structural Engineering, Department of Civil and Architectural Engineering, College of Engineering, Qatar University, P. O. Box 2713, Doha, Qatar.

[*]Corresponding author, e–mail: uebead@qu.edu.qa

[3] Assistant Professor, Department of Civil, Architectural and Environmental Engineering, University of Miami, Coral Gables, FL 33146, USA, e-mail: suranenip@miami.edu

[4] Professor, Department of Civil, Architectural and Environmental Engineering, University of Miami, Coral Gables, FL 33146, USA, e-mail: nanni@miami.edu

Abstract

Combining seawater, recycled coarse aggregate (RCA), and glass fiber reinforced polymer (GFRP) reinforcement in structural concrete is potentially advantageous from a sustainability perspective. This paper reports the results of an experimental study on the flexural performance of seawater-mixed recycled-aggregate concrete beams reinforced with GFRP bars. Twelve medium-scale reinforced concrete (RC) beams ($150 \times 260 \times 2200$ mm) were tested under four-point loading. The test variables included the mixing water (seawater/freshwater), aggregate type (conventional/recycled), and reinforcement material (black steel/GFRP). A wide range of flexural properties, including failure mode, cracking behavior, load-carrying capacity, deformation, energy absorption, and ductility were characterized and compared among the beam specimens. The results suggest that the use of seawater and RCA in concrete has insignificant effects on the flexural capacity of RC beams, especially if concrete strength is preserved by adjusting the mixture design. Altering reinforcement material had a strong influence on the flexural capacity and performance of the tested specimens: the GFRP-RC beams exhibited higher load-carrying capacities (on average 25%) but inferior deformational characteristics as compared to their steel-reinforced counterparts. Theoretical predictions were obtained for the flexural capacity, crack width, and deflection of steel- and GFRP-RC beams based on their corresponding design guides, and compared with the experimental results.

Keywords: Sustainable concrete; GFRP-reinforced concrete; Recycled-aggregate concrete; Seawater-mixed concrete; Flexural performance; Reinforced concrete beams.

1. Introduction

The increasingly global concerns of freshwater scarcity [1], desalination impacts [2], accumulation of construction and demolition wastes [3], possible depletion of natural aggregates [3], and deterioration of reinforced concrete (RC) structures due to steel corrosion [4] impose the need to use alternative "greener" materials [5–9] to achieve more efficient and sustainable RC structures. In an attempt to address these issues, the current paper investigates a seawater-mixed concrete incorporating recycled coarse aggregates (RCA) and corrosion-resistant reinforcement (glass fiber reinforced polymer (GFRP)). Possible corrosion concerns associated with chloride ions in seawater and/or possibly contaminated RCA are avoided through the use of GFRP.

Existing literature postulates direct environmental benefits associated with the use of seawater or RCA in structural concrete. For instance, Arosio et al. [10] reported that mixing concrete with seawater would lead to a reduction up to 12% in its water footprint. Hossain et al. [11] reported that using RCA in concrete mixtures can result in approximately 65% savings in greenhouse gas emissions and up to 58% reductions in the non-renewable energy consumption. These findings have been corroborated by other studies on RCA environmental benefits [12–14]. Studies have shown that GFRP also provides clear environmental benefits in concrete structures due to the increased service life [15–18]. For instance, Cadenazzi et al. [16] reported cradle-to-grave reductions in global warming (by 25%), photochemical oxidant creation (by 15%), acidification (by 5%), and eutrophication (by 50%) when using GFRP rather than black steel to reinforce concrete bridges. Considering these materials together may result in significant economic benefits apart from the environmental benefits. Younis et al. [19] performed a life-cycle cost analysis on seawater-mixed recycled-aggregate GFRP-reinforced concrete for high-rise buildings considering a 100-year service period, and reported approximately 50% long-term cost savings associated with the proposed concrete compared to the traditional counterpart (i.e., concrete with freshwater, conventional aggregate, and steel reinforcement).

Studies on seawater concrete [6,20,21] have generally reported slight reductions in later-age concrete strength (up to 10%) likely due to the presence of certain ions in seawater (although these reductions depend on the curing regime used). However, such reductions can be alleviated by mixture design modifications, including the use of selected chemical admixtures in concrete [22,23]. Durability studies have also verified the long-term strength performance of GFRP bars in seawater concrete [24–26]. Studies on the flexural performance of RC beams with seawater-mixed concrete are limited [27] and rather of durability concern. In this context, Dong et al. [27] reported a change in the failure mode of seawater concrete beams reinforced with steel/FRP composite bars and subject to aggressive exposure (over 6-month immersion in 50 °C seawater) from concrete crushing to rebar tensile rupture, associated with up to 11% reduction in the flexural capacity.

The effects of using RCA on the performance of plain concrete [28–35] as well as flexural performance of RC beams [36–44] are well studied. A complete replacement of natural coarse aggregates (NCA) by RCA in plain concrete results in reductions up to 30% in compressive strength, 24% in tensile strength, and 45% in elastic modulus [29,31,32,34]. Also, using seawater and RCA together at 100% replacement level results in 30–40% reduction in compressive concrete strength [45,46]. However, Alnahhal and Aljidda [36], Sunayana and Barai [37], and other researchers [38–44] reported no significant difference in flexural capacity and service-load deflections between NCA and RCA reinforced concrete beams having the same reinforcement ratio and concrete strength.

GFRP has shown high potential as an alternative non-corrosive reinforcement given its high strength-to-weight ratio [47], excellent durability performance [48], and relatively lower cost compared to carbon FRPs [49]. Design guidelines have also been developed for using GFRP bars in RC elements [50,51], and successful implementation in several types of structures such as bridges [52–54], parking garages [55], tunnels and marine assemblies [56] has been achieved. Research on the flexural performance of GFRP-RC beams [57–66] has demonstrated higher flexural strength but lower stiffness and ductility of GFRP-RC beams compared to their steel-reinforced counterparts, attributable to the linear elastic behavior and the relatively lower elastic modulus of GFRP bars [47].

The main research gap identified from the above literature survey is the lack of understanding of the flexural behavior of seawater-mixed recycled-aggregate GFRP-reinforced concrete beams – which is the aim of the current paper. To achieve this, twelve RC beams with varying concrete mixture design and reinforcement material were constructed and tested under four-point loading.

2. Experimental Program

2.1 Concrete mixtures

Ready-mix concrete, with a 28-day design compressive strength of 60 MPa, was used to cast the RC beam specimens. Three concrete mixtures were considered, as shown in Table 1. Mix A (reference) is the conventional mix with freshwater and NCA. In Mix B, seawater replaced freshwater as mixing water. Mix C represents concrete mixed with seawater and RCA at 100% replacement level. Blast furnace slag was used in all mixtures as supplementary cementitious material (at 65% Portland cement replacement level) as it is known to improve the durability of seawater and/or RCA concrete [20,46]. Chemical and mechanical characterization details for the mix constituents can be found in [22,45].

Table 1 presents the mix proportions (per cubic meter) as per BS EN 206 [67] for each mixture. Direct volume replacement was used to determine the amount of RCA replacing NCA in Mix C

[45]. Additional mixing water was used in Mix C to compensate the higher water absorption of RCA (compared to NCA) [45]. Remedial measures were adopted in Mix B and Mix C to address the performance reductions expected due to the use of seawater and RCA, using chemical admixtures and/or reducing the water-to-cementitious material (w/cm) ratio as detailed in [22,45]. Consequently, Mix B and Mix C concretes showed performance comparable to the conventional Mix A for both workability and strength (Table 1).

2.2 RC beam specimens

Table 2 presents the test matrix for the RC beam specimens used in the current study. Twelve RC beam specimens were tested under four-point loading to assess their flexural performance. Two test variables were considered, namely, the concrete mixture (Mix A, B, or C) and the reinforcement material (steel/GFRP). Two identical samples were tested for each beam specimen. As shown in Figure 1, the beam specimens were 2.2 m in length (L), 150 mm in width (b), and 260 mm in height (h). GFRP/steel bars of 8 mm in diameter were used as transverse and top reinforcement, while 12 mm diameter bars were used as main flexural reinforcement. A 25 mm clear cover to reinforcement was maintained from all sides of the beam specimen, resulting in an effective depth (d) of 221 mm. Steel bars of grade 500B (BS 4449:2005 [70]) were used as reinforcement in steel-RC beam specimens. The yield stress, yield strain, and modulus of elasticity were measured as 594 MPa, 0.27%, and 220 GPa, respectively [71]. The GFRP bars had a tensile modulus of 45 GPa, a guaranteed tensile strength (f_{fu}^{*}) of 760 MPa, and a maximum strain of 1.7% as provided by the manufacturer [72]. It is emphasized that the reinforcement ratio was kept the same among beam specimens with different concrete mixtures, with an intent to investigate the effects of mixing with seawater and RCA.

2.3 Test setup

Figure 2 illustrates the test setup and instrumentation for a typical specimen. After two months following casting, each specimen was tested under four-point bending with monotonic loading using the Instron 1500 HDX Static Hydraulic Universal Testing Machine. Displacement-controlled loading was applied at a rate of 1 mm/min until failure. The vertical deflection at mid-span was monitored using a Linear Variable Displacement Transducer (LVDT). The beam specimen midspan was instrumented with a 60-mm strain gauge bonded at the top concrete surface and with two 5-mm strain gauges bonded to the rebars in tension. Additionally, a clip-type displacement transducer was placed at the side of the beam to measure the crack width as shown in Figure 2. Data acquisition was performed at a frequency of 1 Hz.

3. Experimental Results

Table 3 presents a summary of the experimental results. In general, using seawater and/or RCA in the concrete mix had ultimately little-to-no effect on the flexural performance of RC beams, consistent with previous studies on recycled-aggregate RC beams [36,37]. This is perhaps unsurprising as the workability and strength were comparable among the concrete mixtures (Table 1). Reinforcement material, however, showed a notable effect on the flexural capacity as well as the deformational characteristics of the RC beams tested, conforming with previous studies on FRP-RC beams [57–66]. The following sub-sections (3.1–3.6) provide a detailed discussion on the experimental results.

3.1 Modes of failure

Column 11 of Table 3 presents the failure modes of the tested beams. The concrete mixture had no effect on the flexural failure behavior of RC beams, and the failure was a function of the reinforcement material. Two distinct failure modes were observed, namely, (a) concrete crushing in steel-RC beams (Figure 3) and (b) rebar tensile rupture in GFRP-RC beams (Figure 4). The compression failure mode in steel-RC beams was verified via the concrete compressive strain values at the top surface, which were generally close to or often exceeded the 0.003 maximum strain specified by ACI-318 [73] (Column 5 of Table 3). The tensile failure mode of GFRP-RC beams was confirmed by the rebar tensile strains reaching the ultimate value provided by the supplier ($\varepsilon_{fu}^{*} = 1.7\%$) (Column 4 of Table 3), in addition to the relatively small concrete compressive strains at failure (Column 5 of Table 3).

3.2 Load-carrying capacity

Column 2 of Table 3 lists the values of the load-carrying capacity (P_u) of all beams. The difference in P_u was insignificant ($\leq 5\%$) among the companion specimens with different concrete mixtures. Taking the six steel-RC beams as an example, the two-beam average P_u values were calculated as 84.5, 82.3, and 86.7 kN for Mixes A, B, and C, respectively. As expected, the effect of the reinforcement material was substantial on the flexural capacity of the tested RC beams. The average load-carrying capacity of GFRP- and steel-reinforced concrete beams was 103 and 85 kN, respectively — i.e., the GFRP-RC beams outperformed their steel-reinforced counterparts by approximately 25%. This is attributed to the fact that the reinforcement in GFRP-RC beams had fully attained its tensile strength ($f_{fu}^{*} = 760\ MPa$) at failure, as opposed to their steel-reinforced counterparts whose reinforcement only yielded at $f_y = 594\ MPa$.

3.3 Deformational characteristics

Figures 5-a and 5-b present the load-deflection responses for steel- and GFRP-RC beams, respectively. As shown in Figure 5-a, the load-deflection diagram of steel-RC beams typically consisted of three phases: (a) the uncracked phase, (b) the post-cracking/reduced-stiffness phase, and (c) the yield plateau that had a very small stiffness. On the other hand, the GFRP-RC beams showed a typical bilinear load-deflection response that represented two distinct phases, namely, the uncracked phase and the reduced-slope/post-cracking phase. These observed load-deflection behaviors were the same among beams with different concrete mixtures. Figures 6-a and 6-b show an idealization of the load-deflection response for steel- and GFRP-RC beams, respectively.

The uncracked stiffness (S_i) widely varied among the tested beams without showing a specific pattern with different reinforcements or concrete mixtures, with an overall average of 48.0 kN/mm (compared to an average expected value 56.9 kN/mm). The post-cracking stiffness (S_{cr}) values are listed in Column 9 of Table 3. The post-cracking stiffness of steel-RC beams (6.78 ± 0.64 kN/mm) was higher than that of the GFRP-reinforced counterparts (2.45 ± 0.21 kN/mm), implying that the GFRP-RC beams exhibited higher amounts of deflection at service-load conditions due to the lower tensile modulus of GFRP. No effect of using seawater and/or RCA was observed on the stiffness values of the tested beams.

The deflection values measured at failure (δ_u) for the tested beams are listed in Column 3 of Table 3. GFRP-RC beams had generally lower δ_u values compared to their steel-reinforced counterparts. On average, the maximum deflection measured for GFRP- and steel-reinforced concrete beams was approximately 40 and 50 mm, respectively. This is indeed attributed to the more ductile behavior of steel-RC beams. As shown in Figure 5-a, most of the steel-RC beam's deflection occurred after the steel yielded. The deflection at the yield plateau for steel-RC beams ($\delta_u - \delta_y$) was approximately 86% from the total deflection (δ_u).

3.4 Strain characteristics

The tensile strain of the flexural reinforcement (ε_t), as well as the concrete compressive strain at the top soffit (ε_c), were continuously (and simultaneously) measured at the mid-span of the tested beams, until failure. The maximum tensile (ε_{t-max}) and compressive (ε_{c-max}) strains measured at failure are listed in Columns 4 and 5 of Table 3, respectively. In general, the effect of concrete mix on strain characteristics was negligible when compared to that of the reinforcement material. As expected, steel-RC beams had ε_{t-max} values higher than the yield strain ($\varepsilon_y = 0.27\%$) at failure ($\varepsilon_{t-max} = 1.586\%$ on average), associated with high compressive strains at the top soffit ($\varepsilon_{c-max} = 0.273\%$ on average). The ε_{t-max} values of GFRP-RC beams (1.8% on average) approached or exceeded the ultimate strain value provided by the supplier ($\varepsilon^*_{fu} = 1.7\%$), and were associated with relatively lower ε_{c-max} values (averagely 0.162%) compared to the steel-RC beams. These results taken together confirm the compression failure mode in steel-RC beams as well as the tensile failure mode exhibited by GFRP-RC beam specimens.

Figures 7-a and 7-b depict the increase in the rebar tensile strain with the applied load for steel- and GFRP-RC beams, respectively. In general, the tensile strain of the flexural reinforcement started to significantly develop just after the crack initiation (at $P = P_{cr}$). After that, the tensile strain increased with the applied load, taking a shape matching the constitutive law for the reinforcement material — i.e., linear elastic to failure for GFRP (Figure 7-b) and bi-linear for steel (Figure 7-a). Likewise, Figures 8-a and 8-b present the load versus concrete-compressive-strain diagrams for steel- and GFRP-RC specimens, respectively. In general, the $P - \varepsilon_c$ curves of the tested beams had profiles similar to their load-deflection diagrams (i.e., tri-linear for steel-RC beams and bi-linear for GFRP-RC beam specimens), with approximately the same load values at pivot points.

3.5 Energy absorption

Energy absorption (ψ) is defined as the total area under the load-deflection curve up until the failure point (δ_u, P_u) [74]. Column 10 of Table 3 lists the energy absorption values determined for the beam specimens. The concrete mixture type showed no clear effect on the energy absorption of the tested beams when compared to that of the reinforcement material. The ψ values calculated for steel- and GFRP-RC beam specimens (expressed as average $\pm$ standard deviation) were 3611 $\pm$ 698 and 2468 $\pm$ 588 kN.mm, respectively, indicating the superior flexural performance of the steel-RC beams due to their ductile behavior as demonstrated in load-deflection diagrams (Figure 5). The steel-RC beams exhibited a ductility index (defined here as the ratio of the deflection at ultimate to that at steel yielding) of 6.1 on average.

3.6 Cracking behavior

All beams exhibited a steep load-deflection response until the applied load reached the cracking load (P_{cr}), at which crack initiated at the constant-moment zone of the beam span. Column 6 of Table 3 lists the P_{cr} values for the tested beams. The P_{cr} values ranged from 14.8 kN (Specimen A-F-1) to 22.2 kN (Specimen B-S-1), with an average value of 19.0 kN and a standard deviation of 2.3 kN. No clear or patterned effect of the concrete mix was observed on P_{cr} (given that $f_{c'}$ was comparable among concrete mixtures), and the cracking pattern was almost the same among specimens with different concrete mixtures.

The reinforcement material exhibited a clear effect on the cracking behavior of the tested specimen. Figures 9-a and 9-b present the cracking pattern for steel- and GFRP-RC beams, respectively. While, both steel- and GFRP-RC beams showed a flexural-shear crack pattern that is naturally expected for an RC beam subject to 4-point loading, the former had generally a greater number of cracks at failure (see Figure 9-a and Column 7 of Table 3). Furthermore, the crack-width values at failure (w_u) corresponding to steel-RC beams were higher than those of GFRP-reinforced counterparts (Column 8 of Table 3): the average w_u obtained for steel- and GFRP-RC beams was 4.04 and 1.72 mm, respectively. This can be attributed to the fact that the steel yields at the crack location allowing the cracks to widen (bearing in mind the expected better bond between steel bars and concrete). The effect of the beam ductility on the crack width can be demonstrated comparing the $P-w$ diagrams between steel- and GFRP-RC beam specimens (Figure 10-a and 10-b, respectively). Most of the increase in the crack width (approximately 90%) in the steel-RC beams had occurred after the steel yielded (Figure 10-a). Against this, the crack width (following P_{cr}) of GFRP-RC beams had a linear profile (Figure 10-b).

4. Theoretical formulations

4.1 Cracking and ultimate loads

Theoretical values of cracking load (P_{cr-Th}) were obtained considering a concrete modulus of rupture (f_r) determined as per ACI-318 [73] ($f_r = 0.62\sqrt{f_c{'}}$), and accounting for the reinforcement stiffnesses in the gross moments of inertia. As shown in Column 4 of Table 4, the experimental P_{cr} values were lower (by 20% on average) than those predicted using ACI-318 [73].

Theoretical values of load-carrying capacity (P_{u-Th}) were obtained according to ACI 318 [73] for steel-RC beams and ACI 440.1 [50] for GFRP-RC beams. Based on the equilibrium illustrated in Figure 11, the moment capacity (M_n) of a typical steel-RC beam is obtained using Eq. (1):

$$M_n = T\left(d - \frac{\beta_1 c}{2}\right) \qquad vvv(1)$$

where β_1, α_1, and ε_c (see Figure 11) were taken as 0.65, 0.85, and 0.003, respectively, in accordance with ACI 318 provisions [73]. The same formula was used to calculate P_{u-Th} for GFRP-RC beams considering the GFRP tensile parameters ($E_f = 45\ GPa$ and $f_{fu} = f_{fu}^{*} = 760\ MPa$). The concrete compressive strain (ε_c), the depth of compression zone (c), and the rectangular stress block parameters (β_1 and α_1) were obtained by means of "equilibrium and compatibility" as per ACI 440.1 [50] provisions (for tension-controlled failure).

Columns 6 and 7 of Table 4 list P_{u-Th} values and P_u/P_{u-Th} ratios for the tested RC beams, respectively. The experimental values of load-carrying capacity were generally higher (except for C-F-1) than those predicted by the ACI design guides [50,73]. A reasonable agreement was obtained between the experimental and theoretical P_u values, with an approximate average difference of 7.5%.

4.2 Crack width

The ACI-318 design code [50] accounts for the crack-width control of steel RC beams by setting maximum limits for the reinforcement spacing, rather than using a specific formula to calculate the crack width. ACI 440.1 [75], however, recommends using Eq. (2) to calculate the maximum crack width for FRP-RC beams under flexure.

$$w = 2\frac{f_f}{E_f}\beta k_b\sqrt{d_c^2 + (s/2)^2} \quad (2)$$

where w is the maximum crack width (in mm); f_f is the reinforcement stress (in MPa); E_f is the reinforcement modulus of elasticity (in MPa); β is the ratio of the distance between neutral axis and extreme tension face to the distance between neutral axis and centroid of reinforcement; d_c is the thickness of cover from the extreme tension face to the center of closest bar (in mm); s is the bar spacing (in mm); and k_b is a coefficient that indicates the degree of bond between FRP bar and concrete. In accordance with ACI 440.1 [75], k_b was conservatively taken here as 1.4 given the lack of experimental evidence on the bond between concrete and the GFRP bars used here.

Columns 11–13 of Table 4 compare the predicted and experimental values of crack width at service load. The service load (P_{ser}) for GFRP-RC beams refers to the load at which the rebar tensile stress reaches the creep-rupture limit ($f_f = 0.3f_{fu}$ [76]), and was determined to be 30.2 kN. The small difference in f_c' among the concrete mixtures had ultimately no effect on crack-width calculations. The predicted crack width at service load (w_{ser-Th}) was calculated as 0.90 mm, and was generally higher than that experimentally measured (0.60 mm on average). This discrepancy is probably attributed to the conservative use of $k_b = 1.4$. Considering a k_b of 1.2 (as recommended by ISIS [77]) reduced the gap between the predicted and experimental w_{ser} values by 40%.

Likewise, the crack width was predicted for steel-RC beams using Eq. (2) considering the tensile parameters of steel bars and taking k_b as 1.0 [75]. The stress level at steel bars was taken as $0.4f_y$ (adopted in the allowable stress method [78]) and corresponded to $P_{ser} = 30.0\ kN$. The w_{ser} for steel-RC was predicted as 0.14 mm (compared to an average experimental value of 0.17). The discrepancy observed among steel-RC beams in the experimental w_{ser} are likely attributed to deviations in their uncracked stiffness.

4.3 Deflection

The immediate mid-span deflection (δ_{Th}) of a simply supported RC beam subject to four-point loading is calculated as follows:

$$\delta = \frac{Pa}{48E_cI_e}(3L^2 - 4a^2) \tag{3}$$

Where L is the total span length; a is the shear span; P is the total applied load; E_c is the concrete modulus of elasticity determined as $E_c = 4700\sqrt{f_c{}'}$ [50]; and I_e is the effective moment of inertia. Prior to concrete crack, I_e is taken as the gross moment of inertia (I_g) that accounts also for reinforcement stiffness. The moment of inertia corresponding to a fully-cracked section (I_{cr}) is calculated using an elastic analysis for the beam section in which the concrete in tension is neglected [73]. During the service-load stage, I_e is calculated to represent the transition between I_g and I_{cr}. The ACI 318 [73] adopts Branson's model [79] to calculate I_e as follows:

$$I_e = \left(\frac{M_{cr}}{M_a}\right)^3 I_g + \left(1 - \left(\frac{M_{cr}}{M_a}\right)^3\right) I_{cr} \tag{4}$$

Where M_a is the applied moment and M_{cr} is the cracking moment.

An alternative formula was suggested by Bischoff [80] to calculate I_e as follows:

$$I_e = \frac{I_{cr}}{1 - (1 - \frac{I_{cr}}{I_g})\left(\frac{M_{cr}}{M_a}\right)^2} \tag{5}$$

Figure 12-a presents the predicted load-deflection response for steel-reinforced specimens (up until $P_{ser} = 30.0\ kN$), obtained using both Branson and Bischoff formulas. The latter appears to have a better match with the experimental $P - \delta$ diagrams, for which an acceptable agreement was obtained, particularly in Specimens C-S-1 and B-S-1 (Column 10 of Table 4). A high discrepancy was observed, though, between the predicted and experimental deflections for the other steel-RC beams, likely attributed to deviations in the uncracked stiffness.

For FRP-RC beams, ACI-440.1R-06 [75] had recommended the use of an adjusted form of Branson's formula to calculate I_e as follows:

$$I_e = \left(\frac{M_{cr}}{M_a}\right)^3 \beta_d I_g + \left(1 - \left(\frac{M_{cr}}{M_a}\right)^3\right) * I_{cr} \qquad (6)$$

Where $\beta_d = 0.2\rho_f/\rho_{fb}$ is a reduction coefficient related to the reduced tension stiffening of FRP-RC beams. Lately, the ACI-440.1R-15 [50] design guide replaced Eq. (6) with an updated form of Bischoff's formula to calculate I_e as follows:

$$I_e = \frac{I_{cr}}{1 - \gamma(1 - \frac{I_{cr}}{I_g})\left(\frac{M_{cr}}{M_a}\right)^2} \qquad (7)$$

Where γ (function of a/L and M_{cr}/M_a [50]) is a factor that accounts for the variation in stiffness along the beam span, calculated here as $\gamma = 1.85 - 0.85\frac{M_{cr}}{M_a}$.

The design manual ISIS-2007 [77] recommends using Eq. (8) to calculate I_e as follows:

$$I_e = \frac{I_{cr} I_g}{I_{cr} + \left(1 - 0.5\left(\frac{M_{cr}}{M_a}\right)^2\right)\left(I_g - I_{cr}\right)} \tag{8}$$

The CSA S806-12 [51] design code recommends using Eq. (9) to calculate the deflection of a simply supported beam subject to 4-point loading, as follows:

$$\delta = \frac{PL^3}{48E_c I_{cr}}\left(3\frac{a}{L} - 4\left(\frac{a}{L}\right)^3 - 8\left(1 - \frac{I_{cr}}{I_g}\right)\left(\frac{L_g}{L}\right)^3\right) \tag{9}$$

Where $L_g = aM_{cr}/M_a$ is the length of the uncracked section.

Figure 12-b compares the predicted load-deflection responses among the aforementioned design codes for GFRP-reinforced specimens (up until $P_{ser} = 30.2\ kN$). Compared to the experimental $P - \delta$ diagrams, the ACI-440.1R-06 formula [75] appeared to be the most representative to the tested specimens, while the CSA S806-12 [51] formula was the most conservative.

Columns 8–10 of Table 4 compare the predicted service deflections (δ_{ser-Th}) with those experimentally measured at P_{ser}. The stipulated δ_{ser-Th} values are those corresponding to Eq. (5) (Bischoff formula [80]) for steel-RC beams and to Eq. (6) (ACI-440.1R-06 [75]) for GFRP-RC beams. A reasonable agreement was obtained between the experimental and predicted δ_{ser} values for GFRP-RC beams, with an approximate average difference of 13%.

5. Summary and conclusions

This paper investigated the flexural performance of seawater-mixed recycled-aggregate GFRP-reinforced concrete beams. Twelve medium-scale RC beams were tested under four-point loading considering three test variables, namely, mixing water (seawater/freshwater), aggregates type (virgin/recycled), and reinforcement material (black steel/GFRP). Based on the study results, the following conclusions have been drawn:

- If reductions in concrete performance are averted (using admixtures and/or changes in concrete mix design), using seawater and recycled coarse aggregate in concrete mixtures has little-to-no effect on the short-term flexural capacity of RC beams. The reinforcement material controls the flexural performance of RC beams.
- Steel-RC beams generally failed due to concrete crushing (i.e., compression failure). The GFRP-RC beams showed a more brittle failure due to rebar tensile rupture. On average, GFRP-RC beams showed approximately 25% increase in the load-carrying capacity as compared to their steel-reinforced counterparts, but they also showed notable reductions in deformational and cracking performance.
- Theoretical values of flexural capacity, deflection, and crack width were predicted for the tested specimens and compared with the experimental results. A reasonable agreement was obtained between the predicted and experimental values of flexural capacity (7.5% difference on average). The predicted deflections of GFRP-RC beams somewhat conformed with the experimental values (averagely 13% difference). Some deviations were observed, though, in crack-width and deflection predictions for certain specimens, mostly attributed to discrepancies in the uncracked stiffness.

Acknowledgment

This effort was made possible by the NPRP grant # NPRP 9-110-2-052 from the Qatar National Research Fund (a member of Qatar Foundation). Special thanks are due to ATP Construction Composites for providing the GFRP reinforcement used in this research. The authors would like to thank Readymix Qatar (as a part of LafargeHolcim) for providing the expertise that greatly assisted the authors in this research.

References

[1] Mekonnen MM, Hoekstra AY. Four billion people facing severe water scarcity. Science Advances 2016;2:e1500323. doi:10.1126/sciadv.1500323.

[2] Miller S, Shemer H, Semiat R. Energy and environmental issues in desalination. Desalination 2015;366:2–8. doi:10.1016/j.desal.2014.11.034.

[3] Tam VWY, Soomro M, Evangelista ACJ. A review of recycled aggregate in concrete applications (2000–2017). Construction and Building Materials 2018;172:272–92. doi:10.1016/j.conbuildmat.2018.03.240.

[4] Koch G, Varney J, Thompson N, Moghissi O, Gould M, Payer J. International Measures of Prevention , Application , and Economics of Corrosion Technologies Study (IMPACT). 2016.

[5] Lee LS, Jain R. The role of FRP composites in a sustainable world. Clean Technologies and Environmental Policy 2009;11:247–9.

[6] Xiao J, Qiang C, Nanni A, Zhang K. Use of sea-sand and seawater in concrete construction: Current status and future opportunities. Construction and Building Materials 2017;155:1101–11. doi:10.1016/j.conbuildmat.2017.08.130.

[7] Senaratne S, Gerace D, Mirza O, Tam VWY, Kang WH. The costs and benefits of combining recycled aggregate with steel fibres as a sustainable, structural material. Journal of Cleaner Production 2016;112:2318–27. doi:10.1016/j.jclepro.2015.10.041.

[8] Bostanci SC, Limbachiya M, Kew H. Use of recycled aggregates for low carbon and cost

effective concrete construction. Journal of Cleaner Production 2018;189:176–96. doi:10.1016/j.jclepro.2018.04.090.

[9] Hosseinzadeh N, Ebead U, Nanni A, Suraneni P. Hydration, Strength, and Shrinkage of Cementitious Materials Mixed with Simulated Desalination Brine. Advances in Civil Engineering Materials 2019;8:20190060. doi:10.1520/acem20190060.

[10] Arosio V, Arrigoni A, Dotelli G. Reducing water footprint of building sector: concrete with seawater and marine aggregates. IOP Conference Series: Earth and Environmental Science 2019;323:12127. doi:10.1088/1755-1315/323/1/012127.

[11] Hossain MU, Poon CS, Lo IMC, Cheng JCP. Comparative environmental evaluation of aggregate production from recycled waste materials and virgin sources by LCA. Resources, Conservation and Recycling 2016;109:67–77. doi:10.1016/j.resconrec.2016.02.009.

[12] Marinković S, Radonjanin V, Malešev M, Ignjatović I. Comparative environmental assessment of natural and recycled aggregate concrete. Waste Management 2010;30:2255–64. doi:10.1016/j.wasman.2010.04.012.

[13] Shan X, Zhou J, Chang VWC, Yang EH. Life cycle assessment of adoption of local recycled aggregates and green concrete in Singapore perspective. Journal of Cleaner Production 2017;164:918–26. doi:10.1016/j.jclepro.2017.07.015.

[14] Butera S, Christensen TH, Astrup TF. Life cycle assessment of construction and demolition waste management. Waste Management 2015;44:196–205. doi:10.1016/j.wasman.2015.07.011.

[15] Chao Z, Wenxiu L, Muhammad A, Lee C. Environmental evaluation of FRP in UK highway bridge deck replacement applications based on a comparative LCA study. Advanced Materials Research 2012;374–377:43–8. doi:10.4028/www.scientific.net/AMR.374-

377.43.

[16] Cadenazzi T, Dotelli G, Rossini M, Nolan S, Nanni A. Life-Cycle Cost and Life-Cycle Assessment Analysis at the Design Stage of a Fiber-Reinforced Polymer-Reinforced Concrete Bridge in Florida. Advances in Civil Engineering Materials 2019;8:20180113. doi:10.1520/ACEM20180113.

[17] Zhang C. Life cycle assessment (LCA) of fibre reinforced polymer (FRP) composites in civil applications. Eco-Efficient Construction and Building Materials: Life Cycle Assessment (LCA), Eco-Labelling and Case Studies, Woodhead Publishing Limited; 2014, p. 565–91. doi:10.1533/9780857097729.3.565.

[18] Chen L, Qu W, Zhu P. Life cycle analysis for concrete beams designed with cross-sections of equal durability. Structural Concrete 2016;17:274–86. doi:10.1002/suco.201400117.

[19] Younis A, Ebead U, Judd S. Life cycle cost analysis of structural concrete using seawater, recycled concrete aggregate, and GFRP reinforcement. Construction and Building Materials 2018;175:152–60. doi:10.1016/j.conbuildmat.2018.04.183.

[20] Nishida T, Otsuki N, Ohara H, Garba-Say ZM, Nagata T. Some considerations for applicability of seawater as mixing water in concrete. Journal of Materials in Civil Engineering 2013;27:B4014004.

[21] Dhondy T, Remennikov A, Shiekh MN. Benefits of using sea sand and seawater in concrete: a comprehensive review. Australian Journal of Structural Engineering 2019:1–10. doi:10.1080/13287982.2019.1659213.

[22] Younis A, Ebead U, Suraneni P, Nanni A. Fresh and Hardened Properties of Seawater-Mixed Concrete. Construction and Building Materials 2018;190:276–86.

[23] Li LG, Chen XQ, Chu SH, Ouyang Y, Kwan AKH. Seawater cement paste: Effects of

seawater and roles of water film thickness and superplasticizer dosage. Construction and Building Materials 2019;229:116862. doi:https://doi.org/10.1016/j.conbuildmat.2019.116862.

[24] El-Hassan H, El-Maaddawy T, Al-Sallamin A, Al-Saidy A. Durability of glass fiber-reinforced polymer bars conditioned in moist seawater-contaminated concrete under sustained load. Construction and Building Materials 2018;175:1–13.

[25] El-Hassan H, El-Maaddawy T, Al-Sallamin A, Al-Saidy A. Performance evaluation and microstructural characterization of GFRP bars in seawater-contaminated concrete. Construction and Building Materials 2017;147:66–78. doi:10.1016/j.conbuildmat.2017.04.135.

[26] Khatibmasjedi M. Sustainable Concrete Using Seawater and Glass Fiber Reinforced Polymer Bars, Ph.D. Thesis. University of Miami, 2018.

[27] Dong Z, Wu G, Zhao XL, Zhu H, Lian JL. Durability test on the flexural performance of seawater sea-sand concrete beams completely reinforced with FRP bars. Construction and Building Materials 2018;192:671–82. doi:10.1016/j.conbuildmat.2018.10.166.

[28] Silva R V., De Brito J, Dhir RK. Fresh-state performance of recycled aggregate concrete: A review. Construction and Building Materials 2018;178:19–31. doi:10.1016/j.conbuildmat.2018.05.149.

[29] Behera M, Bhattacharyya SK, Minocha AK, Deoliya R, Maiti S. Recycled aggregate from C&D waste & its use in concrete - A breakthrough towards sustainability in construction sector: A review. Construction and Building Materials 2014;68:501–16. doi:10.1016/j.conbuildmat.2014.07.003.

[30] Guo H, Shi C, Guan X, Zhu J, Ding Y, Ling TC, et al. Durability of recycled aggregate

concrete – A review. Cement and Concrete Composites 2018;89:251–9. doi:10.1016/j.cemconcomp.2018.03.008.

[31] Kisku N, Joshi H, Ansari M, Panda SK, Nayak S, Dutta SC. A critical review and assessment for usage of recycled aggregate as sustainable construction material. Construction and Building Materials 2017;131:721–40. doi:10.1016/j.conbuildmat.2016.11.029.

[32] Silva R V., De Brito J, Dhir RK. The influence of the use of recycled aggregates on the compressive strength of concrete: A review. European Journal of Environmental and Civil Engineering 2015;19:825–49. doi:10.1080/19648189.2014.974831.

[33] Silva R V., De Brito J, Dhir RK. Prediction of the shrinkage behavior of recycled aggregate concrete: A review. Construction and Building Materials 2015;77:327–39. doi:10.1016/j.conbuildmat.2014.12.102.

[34] Silva R V., De Brito J, Dhir RK. Tensile strength behaviour of recycled aggregate concrete. Construction and Building Materials 2015;83:108–18. doi:10.1016/j.conbuildmat.2015.03.034.

[35] Neves R, Silva A, De Brito J, Silva R V. Statistical modelling of the resistance to chloride penetration in concrete with recycled aggregates. Construction and Building Materials 2018;182:550–60. doi:10.1016/j.conbuildmat.2018.06.125.

[36] Alnahhal W, Aljidda O. Flexural behavior of basalt fiber reinforced concrete beams with recycled concrete coarse aggregates. Construction and Building Materials 2018;169:165–78. doi:10.1016/j.conbuildmat.2018.02.135.

[37] Sunayana S, Barai S V. Flexural performance and tension-stiffening evaluation of reinforced concrete beam incorporating recycled aggregate and fly ash. Construction and

Building Materials 2018;174:210–23. doi:10.1016/j.conbuildmat.2018.04.072.

[38] Arezoumandi M, Smith A, Volz JS, Khayat KH. An experimental study on flexural strength of reinforced concrete beams with 100% recycled concrete aggregate. Engineering Structures 2015;88:154–62. doi:10.1016/j.engstruct.2015.01.043.

[39] Ignjatović IS, Marinković SB, Mišković ZM, Savić AR. Flexural behavior of reinforced recycled aggregate concrete beams under short-term loading. Materials and Structures/Materiaux et Constructions 2013;46:1045–59. doi:10.1617/s11527-012-9952-9.

[40] Knaack AM, Kurama YC. Behavior of reinforced concrete beams with recycled concrete coarse aggregates. Journal of Structural Engineering (United States) 2015;141:B4014009. doi:10.1061/(ASCE)ST.1943-541X.0001118.

[41] Kang THK, Kim W, Kwak YK, Hong SG. Flexural testing of reinforced concrete beams with recycled concrete aggregates. ACI Structural Journal 2014;111:607–16. doi:10.14359/51686622.

[42] Fathifazl G, Razaqpur AG, Isgor OB, Abbas A, Fournier B, Foo S. Flexural performance of steel-reinforced recycled concrete beams. ACI Structural Journal 2009;106:858–67.

[43] Sato R, Maruyama I, Sogabe T, Sogo M. Flexural behavior of reinforced recycled concrete beams. Journal of Advanced Concrete Technology 2007;5:43–61. doi:10.3151/jact.5.43.

[44] Ajdukiewicz AB, Kliszczewicz AT. Comparative Tests of Beams and Columns Made of Recycled Aggregate Concrete and Natural Aggregate Concrete. Journal of Advanced Concrete Technology 2007;5:259–73. doi:10.3151/jact.5.259.

[45] Younis A, Ebead U, Suraneni P, Nanni A. Performance of Sewater-Mixed Recycled-Aggregate Concrete. Journal of Materials in Civil Engineering 2019;In press.

[46] Etxeberria M, Gonzalez-Corominas A, Pardo P. Influence of seawater and blast furnace

cement employment on recycled aggregate concretes' properties. Construction and Building Materials 2016;115:496–505. doi:10.1016/j.conbuildmat.2016.04.064.

[47] Hensher DA. Fiber-reinforced-plastic (FRP) reinforcement for concrete structures: properties and applications. vol. 42. Elsevier; 2016.

[48] D'Antino T, Pisani MA. Long-term behavior of GFRP reinforcing bars. Composite Structures 2019:111283. doi:10.1016/j.compstruct.2019.111283.

[49] Ilg P, Hoehne C, Guenther E. High-performance materials in infrastructure: A review of applied life cycle costing and its drivers - The case of fiber-reinforced composites. Journal of Cleaner Production 2016;112:926–45. doi:10.1016/j.jclepro.2015.07.051.

[50] ACI Committee 440. Guide for the design and construction of structural concrete reinforced with FRP bars (ACI 440.1 R-15). American Concrete Institute; 2015.

[51] Canadian Standards Association. Design and construction of building components with fiber reinforced polymers (CAN/CSA-S806-12). Ontario, Canada: 2012.

[52] Benmokrane B, El-salakawy E, El-ragaby A, Lackey T. Designing and Testing of Concrete Bridge Decks Reinforced with Glass FRP Bars. Journal of Bridge Engineering 2006;11:217–29. doi:10.1061/(ASCE)1084-0702(2006)11:2(217).

[53] Yang ZY, Liu JY, Zhang YD, Qu JB. Flexural Behavior Finite Element analysis of CFRP Reinforced Concrete Bridge Deck with Corrosion and Salt Resistance. Advanced Materials Research, vol. 1004, Trans Tech Publ; 2014, p. 1474–7.

[54] Mara V, Haghani R, Harryson P. Bridge decks of fibre reinforced polymer (FRP): A sustainable solution. Construction and Building Materials 2014;50:190–9. doi:10.1016/j.conbuildmat.2013.09.036.

[55] Ahmed EA, Benmokrane B, Sansfaçon M. Case study: design, construction, and

performance of the La Chancelière parking garage's concrete flat slabs reinforced with GFRP bars. Journal of Composites for Construction 2017;21:05016001. doi:10.1061/(ASCE)CC.1943-5614.0000656.

[56] Mohamed HM, Benmokrane B. Recent field applications of FRP composite reinforcing bars in civil engineering infrastructures. Proc., Int. Conf. ACUN6–Composites and Nanocomposites in Civil, Offshore and Mining Infrastructure, Melbourne, Australia: 2012, p. 14–6.

[57] Fatih I, Ashour AF. Flexural performance of FRP reinforced concrete beams. Composite Structures 2012;94:1616–25. doi:10.1016/j.compstruct.2011.12.012.

[58] Barris C, Torres L, Turon A, Baena M, Catalan A. An experimental study of the flexural behaviour of GFRP RC beams and comparison with prediction models. Composite Structures 2009;91:286–95. doi:10.1016/j.compstruct.2009.05.005.

[59] Gravina RJ, Smith ST. Flexural behaviour of indeterminate concrete beams reinforced with FRP bars. Engineering Structures 2008;30:2370–80. doi:10.1016/j.engstruct.2007.12.019.

[60] Ascione L, Mancusi G, Spadea S. Flexural Behaviour of Concrete Beams Reinforced With GFRP Bars. Strain 2010;46:460–9. doi:10.1111/j.1475-1305.2009.00662.x.

[61] Kassem C, Farghaly AS, Benmokrane B. Evaluation of Flexural Behavior and Serviceability Performance of Concrete Beams Reinforced with FRP Bars. Journal of Composites for Construction 2011;15:682–95. doi:10.1061/(asce)cc.1943-5614.0000216.

[62] Kara IF, Ashour AF, Dundar C. Deflection of concrete structures reinforced with FRP bars. Composites Part B: Engineering 2013;44:375–84. doi:10.1016/j.compositesb.2012.04.061.

[63] Bischoff PH, Gross SP, Asce AM. Design Approach for Calculating Deflection of FRP-Reinforced Concrete. Journal of Composites for Construction 2011;318:490–9.

doi:10.1061/(ASCE)CC.1943-5614.0000195.

[64] Al-Sunna R, Pilakoutas K, Hajirasouliha I, Guadagnini M. Deflection behaviour of FRP reinforced concrete beams and slabs: An experimental investigation. Composites Part B: Engineering 2012;43:2125–34. doi:10.1016/j.compositesb.2012.03.007.

[65] Barris C, Torres L, Comas J, Miàs C. Cracking and deflections in GFRP RC beams: An experimental study. Composites Part B: Engineering 2013;55:580–90. doi:10.1016/j.compositesb.2013.07.019.

[66] El-Nemr A, Ahmed EA, Benmokrane B. Flexural behavior and serviceability of normal-And high-strength concrete beams reinforced with glass fiber-reinforced polymer bars. ACI Structural Journal 2013;110:1077–87.

[67] BS EN 206: Concrete specification, performance, production and conformity. BSI; 2013.

[68] ASTM C143/C143M-15a: Standard Test Method for Slump of Hydraulic-Cement Concrete. ASTM International; 2015.

[69] ASTM International ASTM C39/C39M-16b. Standard test method for compressive strength of cylindrical concrete specimens, ASTM International, West Conshohocken, PA, 2016. 2009.

[70] ISE/104 Committee. BS 4449:2005: Steel for the reinforcement of concrete. Weldable reinforcing steel. Bar, coil and decoiled product. BSI; 2005.

[71] Ebead U, El-Sherif HE. Near surface embedded-FRCM for flexural strengthening of reinforced concrete beams. Construction and Building Materials 2019;204:166–76. doi:10.1016/j.conbuildmat.2019.01.145.

[72] ATP Construction Composites. Data sheet for GFRP rebars 2019. http://www.atp-frp.com/html/products_tds.html#rwb-v.

[73] ACI Committee 318. Building code requirements for structural concrete (ACI 318-14). Farmington Hills, USA: American Concrete Institute; 2014.

[74] Younis A, Ebead U, Shrestha KC. Different FRCM systems for shear-strengthening of reinforced concrete beams. Construction and Building Materials 2017;153:514–26. doi:10.1016/j.conbuildmat.2017.07.132.

[75] ACI Committee 440. Guide for the Design and Construction of Concrete Reinforced with FRP Bars (ACI 440.1 R-06). Farmington Hills, USA: American Concrete Institute; 2006.

[76] Benmokrane B, Brown VL, Mohamed K, Nanni A, Rossini M, Shield C. Creep-Rupture Limit for GFRP Bars Subjected to Sustained Loads. Journal of Composites for Construction 2019;23:1–7. doi:10.1061/(ASCE)CC.1943-5614.0000971.

[77] ISIS Canada Corporation. ISIS Design Manual: Reinforcing concrete structures with fiber reinforced polymers-Design manual No. 3. Manitoba, Canada: 2007.

[78] McCormac J, Brown R. Design of reinforced concrete. John Wiley & Sons; 2005.

[79] Branson D. Deformation of concrete structures. New York: McGraw-Hill; 1977.

[80] Bischoff PH. Reevaluation of deflection prediction for concrete beams reinforced with steel and fiber reinforced polymer bars. Journal of Structural Engineering 2005;131:752–62. doi:10.1061/(ASCE)0733-9445(2005)131:5(752).

Table 1: Concrete mixtures.

Property	Mix A	Mix B	Mix C
1. Concrete mixture proportions			
Water	165 kg/m³ (Freshwater)	165 kg/m³ (Seawater)	200 kg/m³ (Seawater)
Coarse aggregates	Conventional — 700 kg/m³ (Gabbro 20 mm) + 490 kg/m³ (Gabbro 10 mm)	Conventional — 700 kg/m³ (Gabbro 20 mm) + 490 kg/m³ (Gabbro 10 mm)	Recycled concrete — 990 kg/m³ (5-20 mm RCA)
Fine aggregates	750 kg/m³ (Washed sand)	750 kg/m³ (Washed sand)	750 kg/m³ (Washed sand)
Cementitious material	450 kg/m³ OPC (35%) + Slag (65%)	450 kg/m³ OPC (35%) + Slag (65%)	490 kg/m³ OPC (35%) + Slag (65%)
Retarder (CHRYSOPlast CQ240)	-	0.25 L/m³	0.75 L/m³
Super plasticizer (Glenium 110 M)	4.05 L/m³	4.46 L/m³	5.57 L/m³
2. Concrete fresh properties and compressive strength			
Fresh concrete temperature	28.7 °C	30.0 °C	30.0 °C
Initial slump (as per ASTM C143 [68]**)**	250 mm	260 mm	270 mm
Initial slump flow (as per ASTM C143 [68]**)**	610 mm	650 mm	660 mm
28-day compressive strength, f_c' (as per ASTM C39 [69]**)**	$64.1 \pm 0.4\ MPa$	$68.5 \pm 1.0\ MPa$	$59.7 \pm 0.4\ MPa$

Table 2: Test matrix for the RC beams.

Specimen ID	Concrete Mixture	Reinforcement
A-S-1 & A-S-2	Mix A	Steel
B-S-1 & B-S-2	Mix B	Steel
C-S-1 & C-S-2	Mix C	Steel
A-F-1 & A-F-2	Mix A	GFRP
B-F-1 & B-F-2	Mix B	GFRP
C-F-1 & C-F-2	Mix C	GFRP

Table 3: Summary of the test results.

1	2	3	4	5	6	7	8	9	10	11
Specimen	P_u (kN)	δ_u (mm)	ε_{t-max} (%)	ε_{c-max} (%)	P_{cr} (kN)	**No. of cracks (major)**	w_u (mm)	S_{cr} (kN/mm)	ψ (kN.mm)	**Failure Mode**
A-S-1	79.3	50.6	1.49	0.279	19.0	12	3.60	6.5	3497	Concrete crushing
A-S-2	89.6	56.2	-	0.334	20.4	11	4.40	7.1	4314	Concrete crushing
B-S-1	83.5	47.8	1.95	0.243	22.2	12	4.87	6.7	3372	Concrete crushing
B-S-2	81.1	39.0	1.21	0.246	20.6	10	-	6.2	2680	Concrete crushing
C-S-1	87.3	59.1	0.98	0.245	22.1	10	-	7.9	4548	Concrete crushing
C-S-2	86.1	44.6	2.30	0.293	16.7	12	3.30	6.25	3255	Concrete crushing
A-F-1	103.2	36.9	1.79	0.158	14.8	9	1.53	2.3	2181	GFRP rupture
A-F-2	103.2	37.4	1.94	0.151	17.1	8	-	2.4	2277	GFRP rupture
B-F-1	99.7	40.5	1.71	0.156	19.1	9	1.55	2.2	2382	GFRP rupture
B-F-2	116.2	47.5	1.88	0.185	16.7	10	1.93	2.7	3309	GFRP rupture
C-F-1	92.5	30.5	1.82	0.168	20.4	8	1.88	2.4	1674	GFRP rupture
C-F-2	102.4	44.3	1.67	0.153	19.2	9	-	2.7	2986	GFRP rupture

Table 4: Comparison of experimental and theoretical predictions.

1	2	3	4	5	6	7	8	9	10	11	12	13
Specimen	Cracking load			Load-carrying capacity			Deflection (Service)			Crack width (Service)		
	P_{cr} (kN)	P_{cr-Th} (kN)	$\frac{P_{cr}}{P_{cr-\mathrm{Th}}}$	P_u (kN)	P_{u-Th} (kN)	$\frac{P_u}{P_{u-Th}}$	δ_{ser} (mm)	δ_{ser-Th} (mm)	$\frac{\delta_{ser}}{\delta_{ser-TH}}$	w_{ser} (mm)	w_{ser-Th} (mm)	$\frac{w_{ser}}{w_{ser-TH}}$
A-S-1	19.0	24.5	0.78	79.3	78.8	1.006	1.72	1.23	1.40	0.217	0.141	1.539
A-S-2	20.4	24.5	0.83	89.6	78.8	1.137	1.92	1.23	1.56	0.205	0.141	1.454
B-S-1	22.2	25.3	0.88	83.5	79.0	1.057	1.27	1.13	1.13	0.152	0.140	1.078
B-S-2	20.6	25.3	0.81	81.1	79.0	1.027	2.10	1.13	1.88	-	-	-
C-S-1	22.1	23.7	0.93	87.3	78.6	1.111	1.26	1.33	0.95	-	-	-
C-S-2	16.7	23.7	0.70	86.1	78.6	1.095	2.49	1.33	1.87	0.097	0.141	0.688
A-F-1	14.8	23.2	0.64	103.2	97.4	1.060	4.85	6.06	0.80	0.505	0.905	0.558
A-F-2	17.1	23.2	0.74	103.2	97.4	1.060	5.52	6.06	0.91	-	-	-
B-F-1	19.1	24.0	0.80	99.7	96.4	1.034	5.02	5.69	0.88	0.499	0.904	0.551
B-F-2	16.7	24.0	0.70	116.2	96.4	1.205	5.87	5.69	1.03	0.571	0.904	0.631
C-F-1	20.4	22.4	0.91	92.5	98.5	0.939	5.57	6.45	0.86	0.719	0.905	0.794
C-F-2	19.2	22.4	0.86	102.4	98.5	1.040	5.08	6.45	0.79	-	-	-

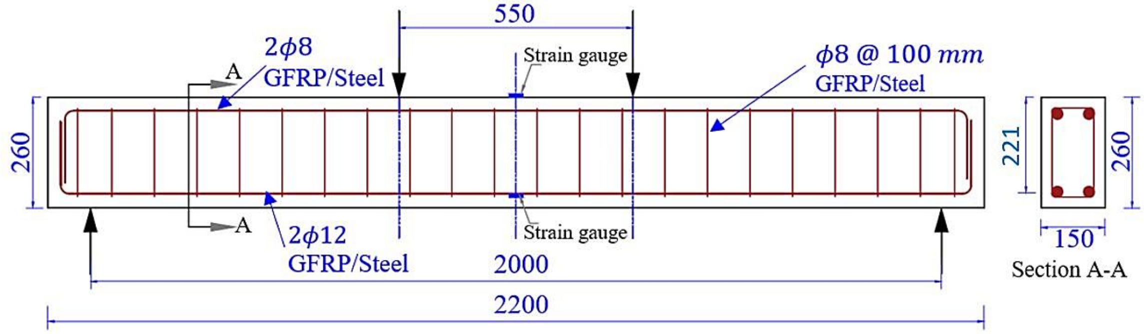

Figure 1. Schematic drawing for a typical RC beam used in this study.

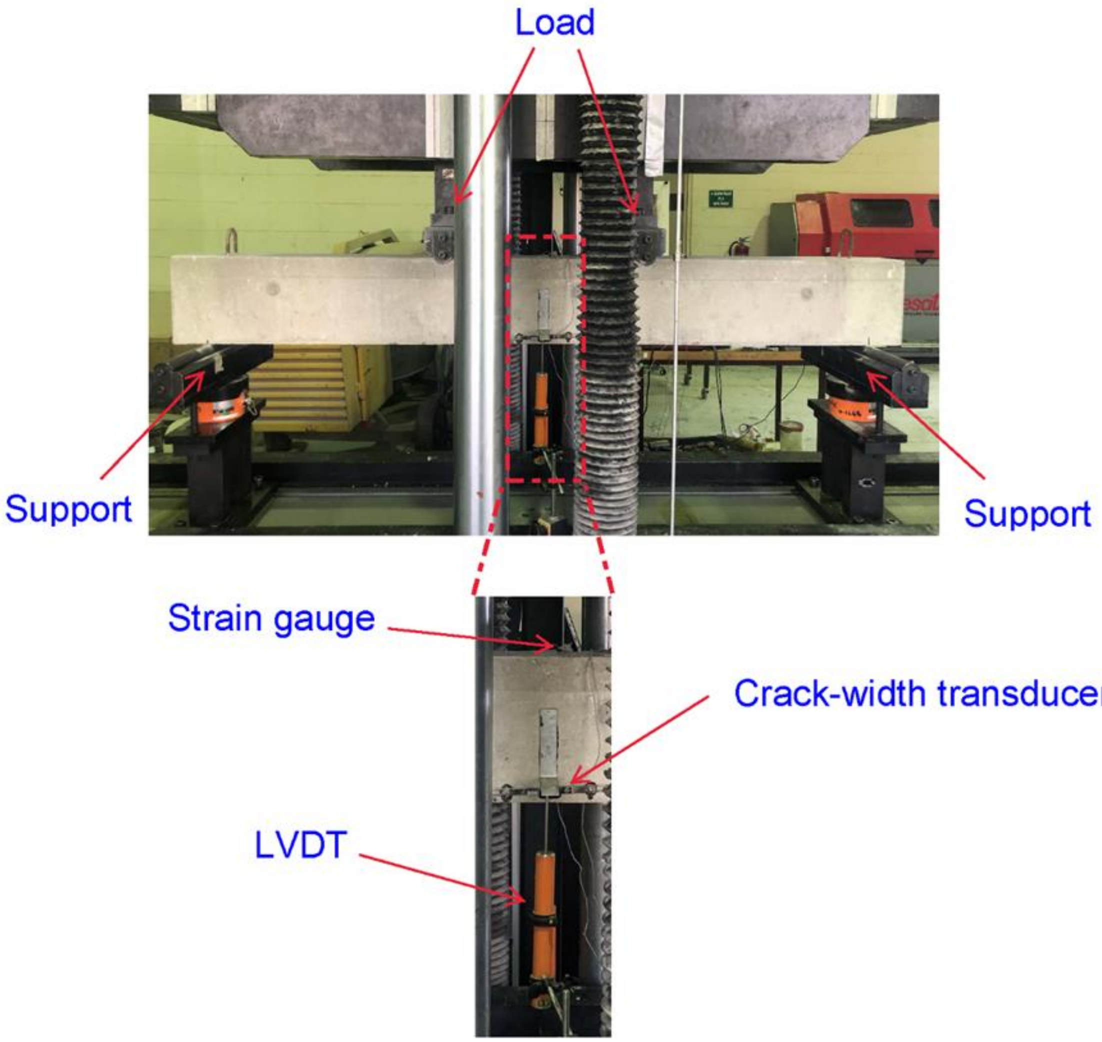

Figure 2. Test setup and instrumentation.

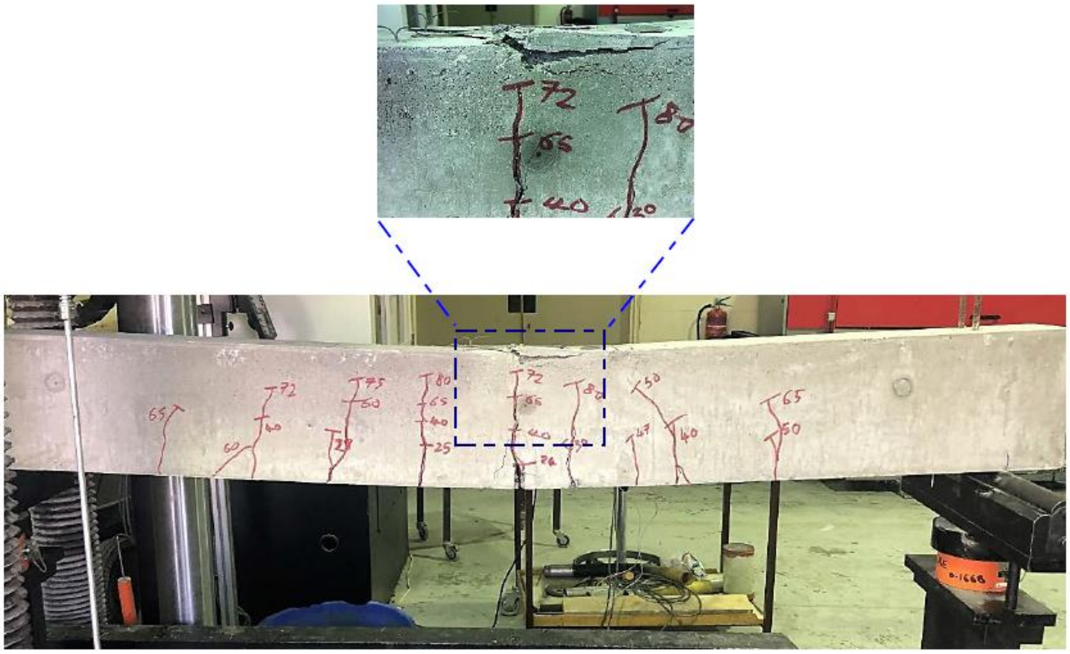

Figure 3. Concrete crushing in Specimen B-S-2.

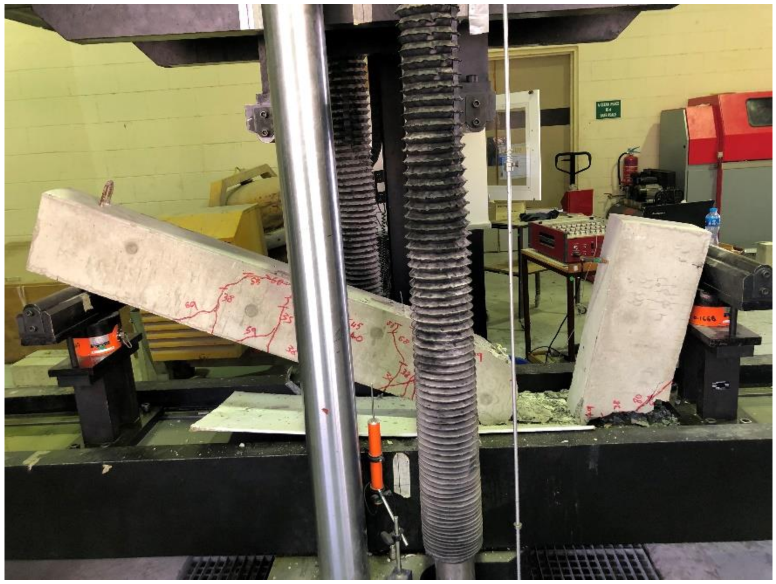

Figure 4. GFRP tensile rupture in Specimen B-F-2.

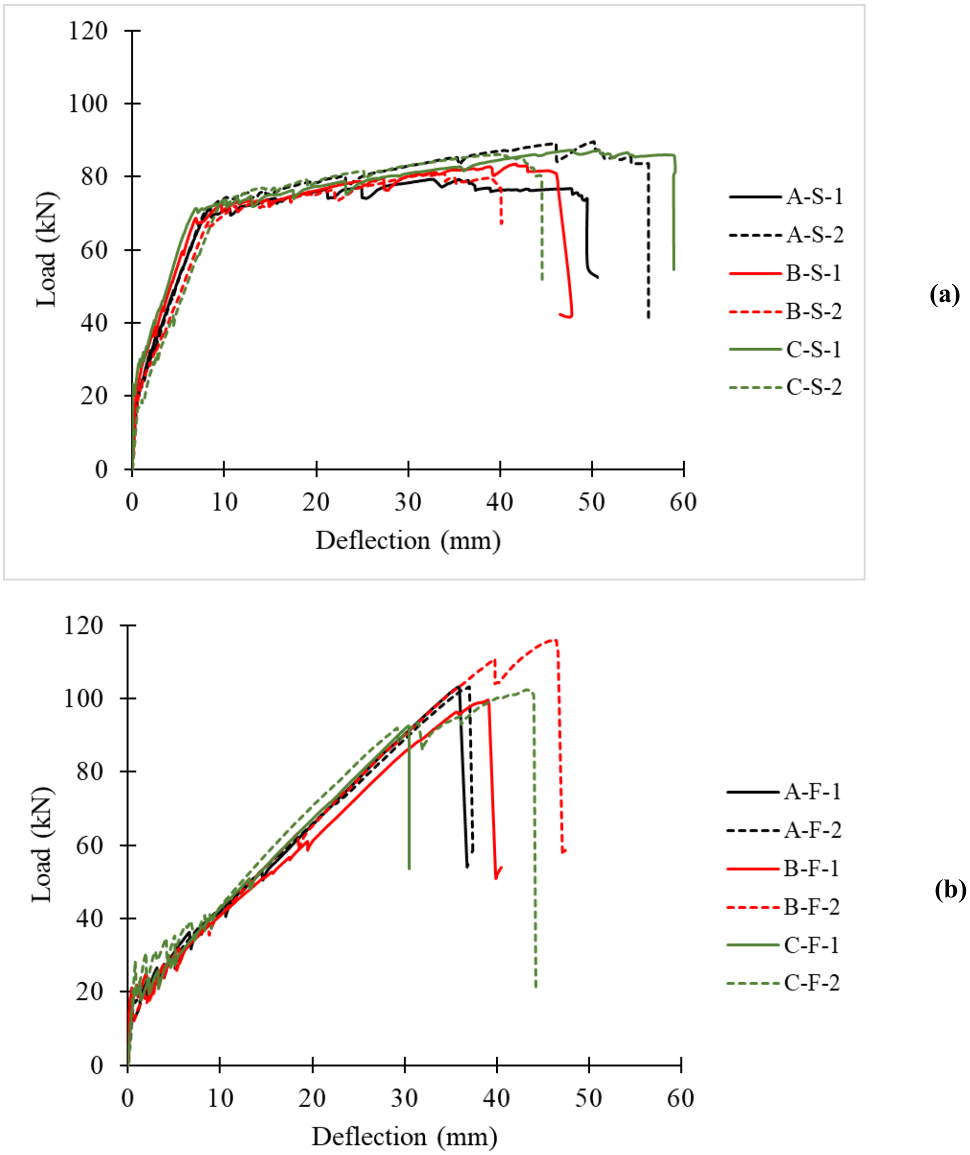

Figure 5. Load vs. deflection diagrams for (a) steel and (b) GFRP reinforced concrete beams.

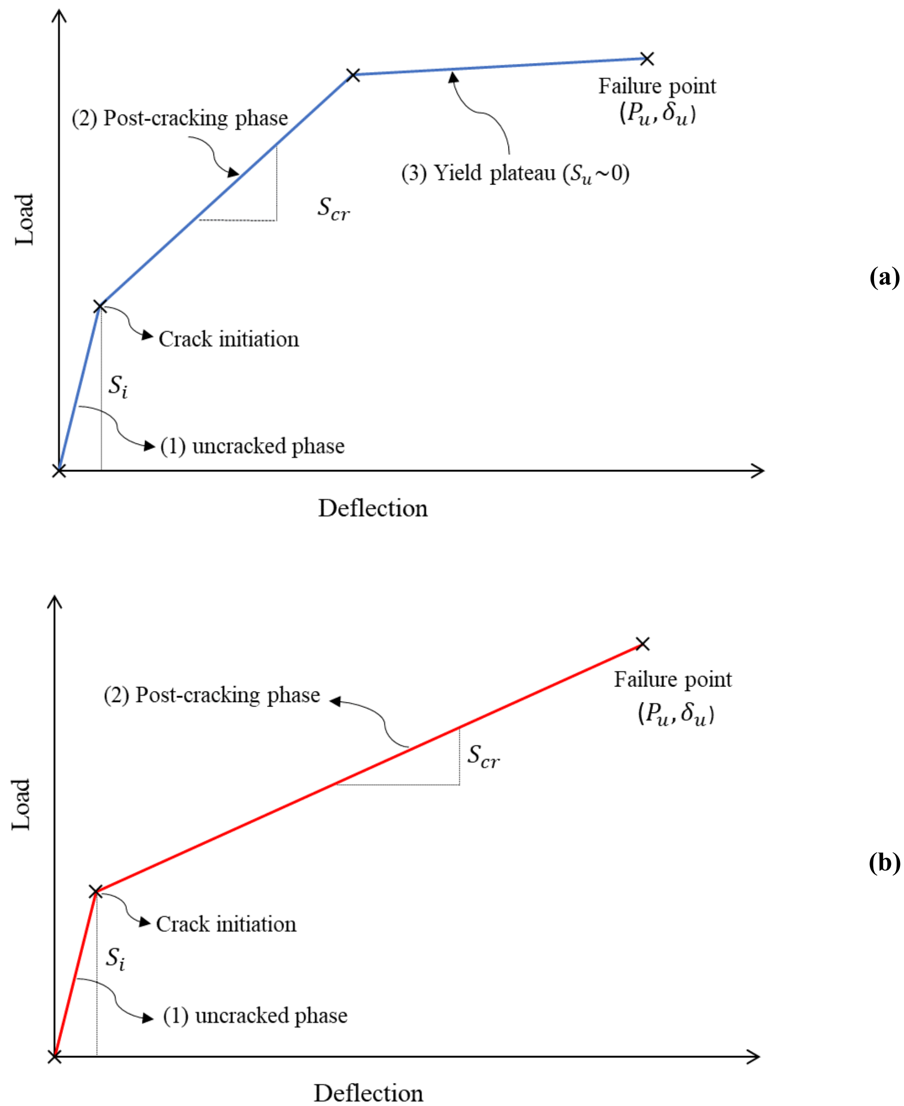

Figure 6. Idealization of load-deflection diagrams for (a) steel and (b) GFRP reinforced concrete beams.

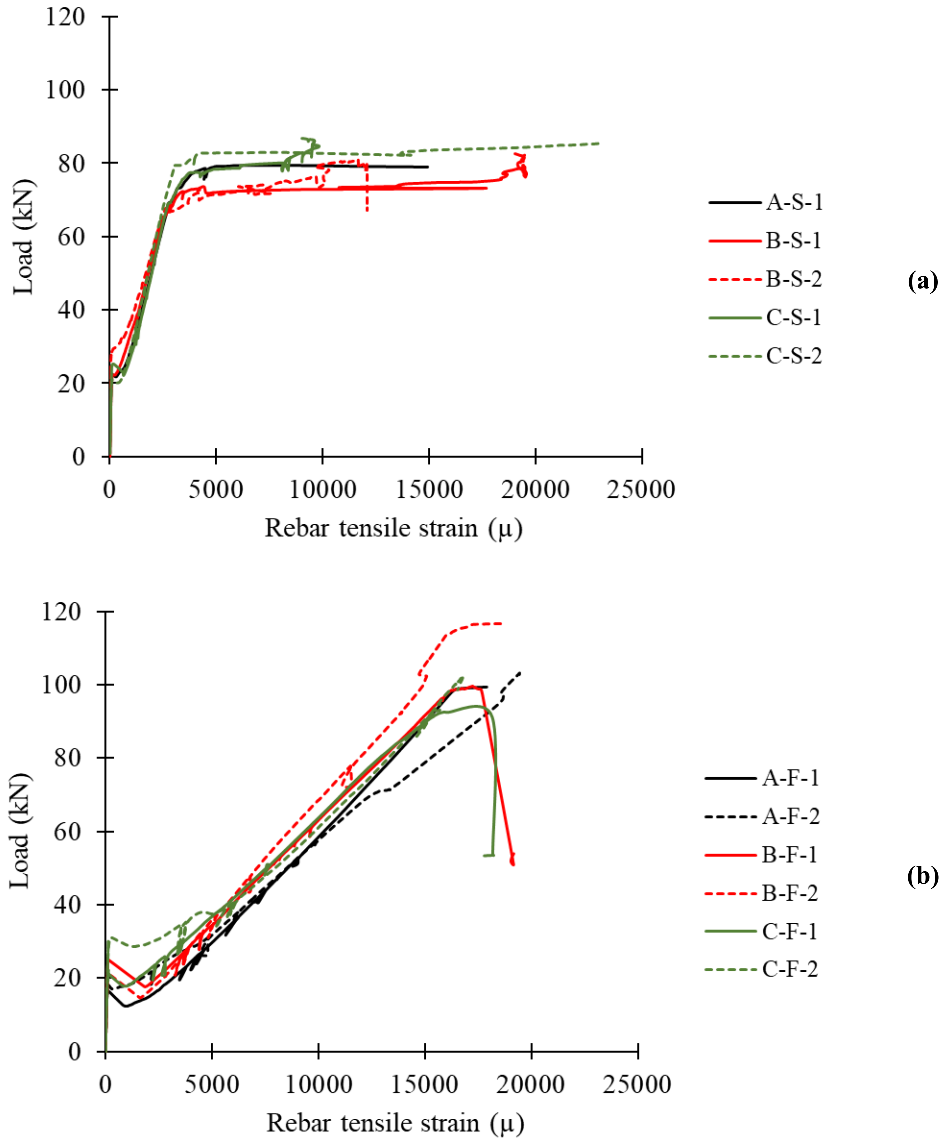

Figure 7. Load vs. rebar strain diagrams for (a) steel and (b) GFRP reinforced concrete beams.

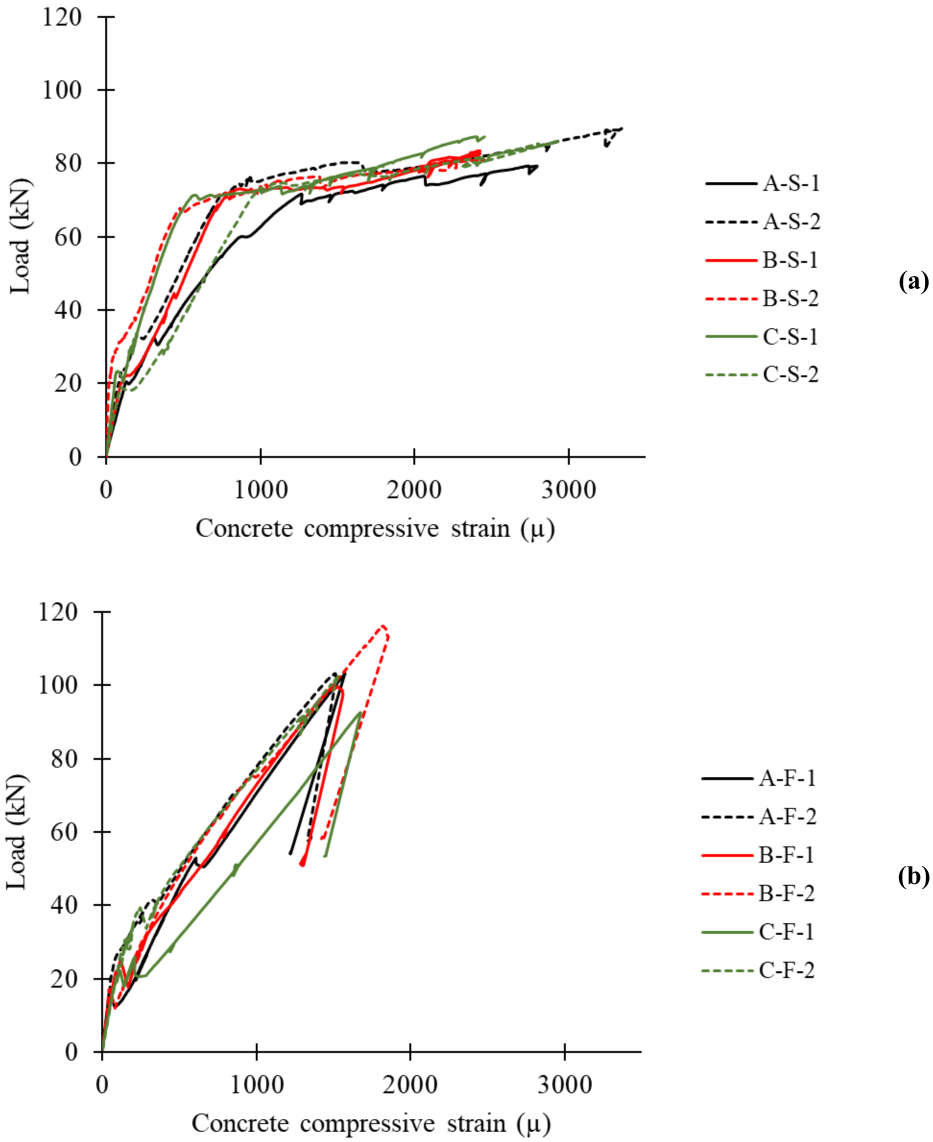

Figure 8. Load vs. concrete compressive strain diagrams for (a) steel and (b) GFRP reinforced concrete beams.

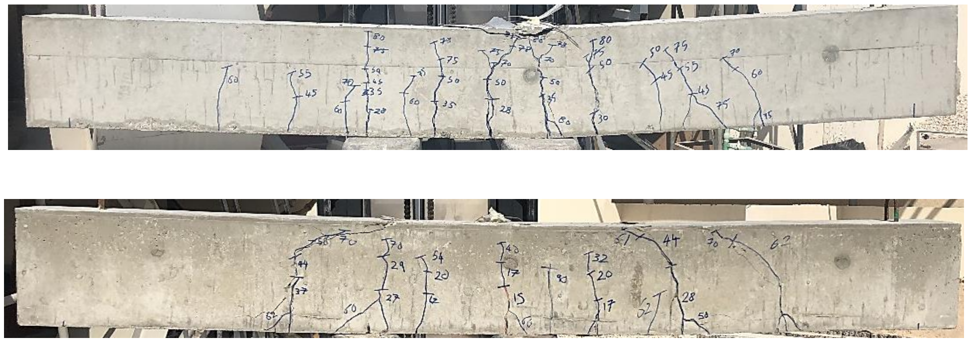

(a)

(b)

Figure 9. Cracking pattern for (a) Specimen C-S-2 and (b) Specimen C-F-2.

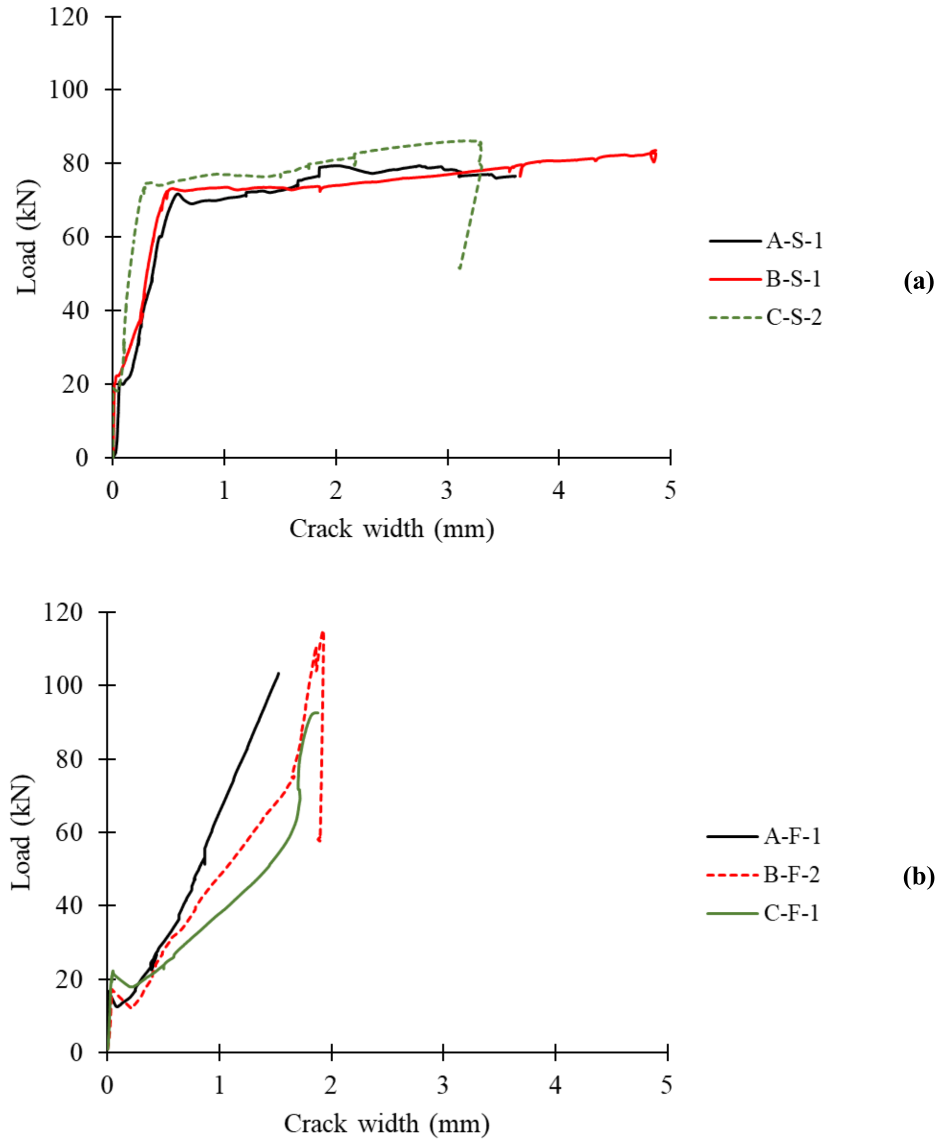

Figure 10. Load vs. crack-width diagrams for samples of (a) steel and (b) GFRP reinforced concrete beams.

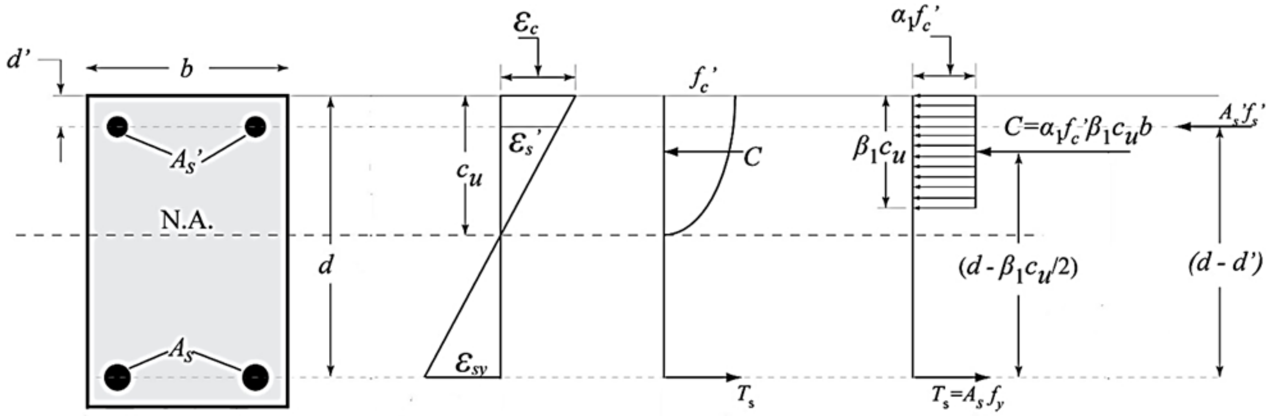

Figure 11. Equilibrium forces for a typical RC beam under flexure.

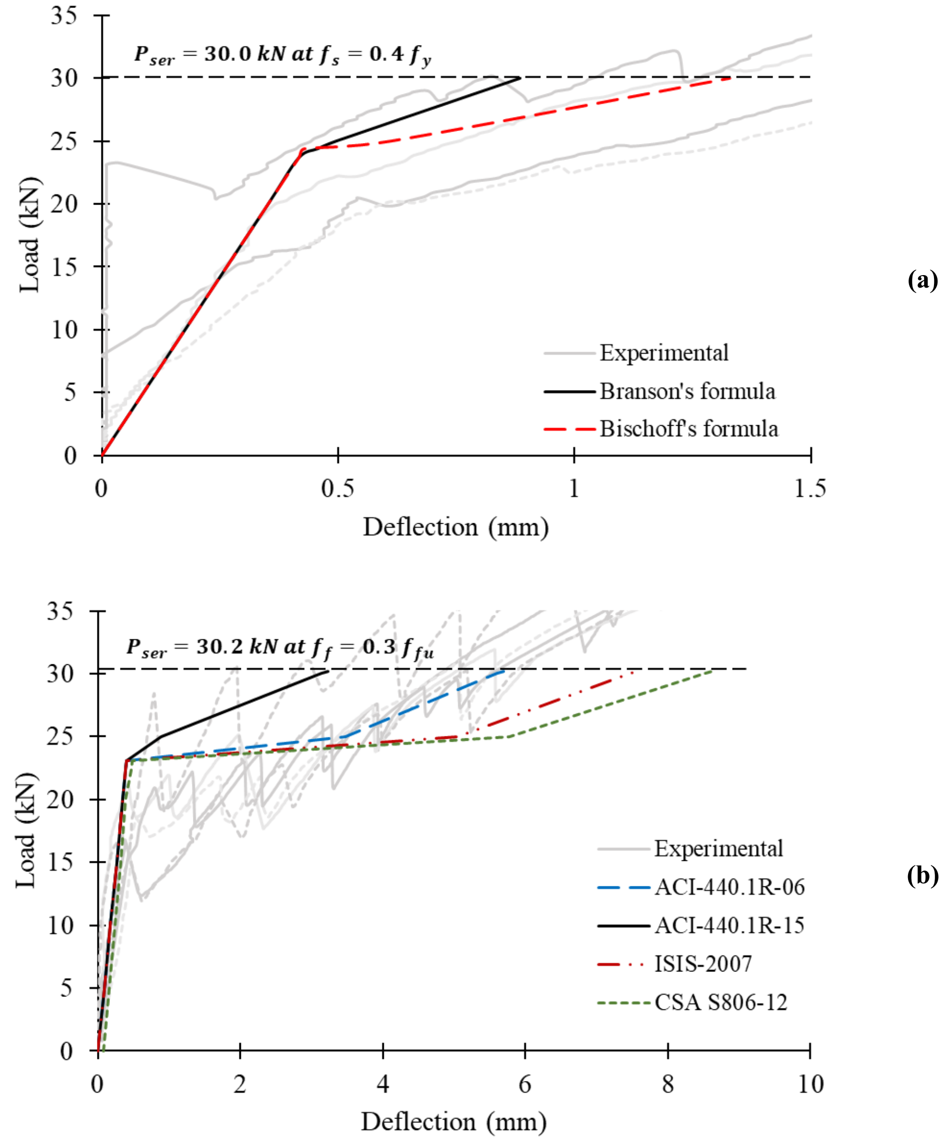

Figure 12. Predicted vs. experimental load-deflection diagrams (taking fc'=60 MPa) for (a) steel-RC and (b) GFRP-RC beams.